The thermal conductivity of unlithified granular volcanic materials: the influence of hydrothermal alteration and degree of water saturation

Michael J. Heap[1,2]*, Fabian B. Wadsworth[3], and David E. Jessop[4,5]

[1] *Université de Strasbourg, CNRS, Institut Terre et Environnement de Strasbourg, UMR 7063, 5 rue Descartes, Strasbourg F-67084, France*

[2] *Institut Universitaire de France (IUF), Paris, France*

[3] *Earth Sciences, Durham University, Science Labs, Durham, DL1 3LE, United Kingdom*

[4] *Université de Paris, Institut de Physique du Globe de Paris, CNRS UMR 7154, F-75005 Paris, France*

[5] *CNRS, IRD, OPGC Laboratoire Magmas et Volcans, Université Clermont Auvergne, F-63000, Clermont-Ferrand, France*

*Corresponding author: Michael Heap (heap@unistra.fr)

Highlights

- Thermal properties of volcanic rocks are typically higher than for unlithified volcanic materials.
- Thermal conductivity and diffusivity of unlithified volcanic material decreases with alteration.
- Thermal conductivity of unlithified volcanic material increases with water saturation degree.
- Thermal conductivity of saturated unlithified volcanic material can be higher than that for dry volcanic rocks.
- Lithification (rock versus powder), alteration, and water saturation degree are important considerations for heat flux calculations.

Abstract

The thermal properties of volcanic materials are required for modelling and for understanding volcanic surface heat fluxes and timescales for cooling magma. However, compared to volcanic rocks, there are relatively few thermal property data for unlithified granular volcanic materials. Here, we measured the thermal properties of a suite of hydrothermally altered powders from La Soufrière de Guadeloupe (Eastern Caribbean) as a function of

water saturation degree. Our data show, under dry conditions, that thermal conductivity and thermal diffusivity decrease, and that specific heat capacity does not change systematically, as a function of the degree of alteration of the unlithified granular material. For example, thermal conductivity decreases from ~0.3 to ~0.2 $W \cdot m^{-1} \cdot K^{-1}$ as the quantity of alteration minerals in the samples increases from ~10 to ~70 wt%. We interpret the decrease in thermal conductivity with increasing alteration as the result of the lower thermal conductivity of the alteration mineral assemblage relative to the unaltered assemblage. Our data also show that thermal conductivity increases from ~0.2–0.3 to ~0.8–1.1 $W \cdot m^{-1} \cdot K^{-1}$ as saturation degree increases from dry to at, or close to, complete saturation, due to the higher thermal conductivity of water compared to air. We show that an empirical model for variably saturated granular media is in general agreement with our data and provides a framework to predict the thermal conductivity of unlithified granular volcanic materials as a function of saturation degree. The data and modelling provided herein can help improve heat flux calculations designed to inform on volcanic and geothermal processes.

Keywords: volcano; thermal conductivity; thermal diffusivity; specific heat capacity; porosity; La Soufrière de Guadeloupe; hydrothermal alteration; saturation; heat flux

1 Introduction

The fragmentation and granulation of magma and volcanic rock is a consequence of the energetic phenomena that often typify active volcanoes. First, explosions, explosive eruptions, directed blasts, and lava fountains, create and expel pyroclasts at various velocities and to various distances (Heiken and Wohletz, 1991; Kueppers et al., 2006) and/or form breccia-filled conduits and brecciated conduit margins (Rust et al., 2004; Goto et al., 2008; Kolzenburg et al., 2014; Kennedy et al., 2020). Even effusive silicic volcanism is thought to be rooted in fragmentation (Wadsworth et al., 2020). Second, the collapse of a lava dome or volcanic flank can form pyroclastic density currents, mixtures of pyroclasts and gas, that sweep across the landscape (Branney et al., 2002; Dufek et al., 2015). These phenomena, and others, can create thick and voluminous layers of granular material that either remain unlithified or, if the pyroclasts are glassy and remain hot, can weld to reform rock (Pyle, 1989; Brown and Andrews, 2015). The net result is a volcanic environment characterised by both lithified rock (lavas and welded granular rocks) and unlithified loose granular material.

The heat from subsurface magma is transported to the surface by hot convecting fluids (hydrothermal systems), the conduction of heat through the edifice (rock and unlithified granular material), and the upward

movement of the magma itself. As a result, active volcanoes are often associated with regions of high surface heat flux (Wright and Flynn, 2004) and, because surface heat flux changes are indicative of the subsurface movement of magma and/or hydrothermal fluids, an increase in surface heat flux can indicate volcanic unrest and perhaps impending eruptive activity (Girona et al., 2021). It is for this reason that surface heat flux is widely used as a monitoring tool at active volcanoes worldwide (Harris et al., 1997; Wooster and Rothery, 1997; Harris et al., 2001; Dehn et al., 2000; Wright et al., 2004; Chiodini et al., 2005; Stevenson and Varley, 2008; Bloomberg et al., 2014; Chiodini et al., 2015; Mannini et al., 2019; Jessop et al., 2020). Understanding the thermal properties of the volcanic edifice, and the processes that can influence these properties, is important for the interpretation of surface heat flux data and can therefore help improve the reliability of volcano monitoring. The thermal properties of volcanic materials are also required in a variety of models designed to estimate timescales for the cooling of magma bodies, dykes, sills, lavas, and ignimbrites (Irvine, 1970; Norton and Knight, 1977; Carrigan, 1984; Bruce and Huppert, 1989; Carrigan et al., 1992; Fialko and Rubin, 1999; Wooster et al., 1997; Annen et al., 2008; Nabelek et al., 2012; Heap et al., 2017; Annen, 2017; Mattsson et al., 2018; Tsang et al., 2019).

Experimental studies have provided values for the thermal properties of volcanic rocks for modelling (Horai et al., 1970; Fujii and Osako, 1973; Robertson and Peck, 1974; Bagdassarov and Dingwell, 1994; Whittington et al., 2009; Romine et al., 2012; Mielke et al., 2015, 2016, 2017; Vélez et al., 2018; Heap et al., 2020; Weydt et al., 2021; Heap et al., 2022a). These studies, and others, have shown that porosity plays a first-order role in dictating thermal properties of volcanic rocks. For example, the thermal conductivity of basalt from Hawai'i (USA) decreased from ~1.7 $W \cdot m^{-1} \cdot K^{-1}$ at a porosity of 0.05 to ~0.2 $W \cdot m^{-1} \cdot K^{-1}$ at a porosity of 0.85 (Robertson and Peck, 1974). The thermal properties of volcanic rocks are also influenced by factors such as temperature, saturation with water, and hydrothermal alteration. For example, the thermal diffusivity of rhyolite decreased from ~2.0 to ~0.7 $mm^2 \cdot s^{-1}$ as temperature was increased from ~260 to ~850 K (Whittington et al., 2009). The thermal conductivity of andesite from Ruapehu (New Zealand) with a porosity of ~0.3 was increased from ~0.8 to ~1.3 $W \cdot m^{-1} \cdot K^{-1}$ upon complete saturation with water (Heap et al., 2020), and hydrothermal alteration has been shown to either increase or decrease the thermal properties of volcanic rocks, depending on whether the alteration was manifest as (1) dissolution and/or replacement or (2) the precipitation of minerals within the void space within the rock (Heap et al., 2022a).

Although data exist for volcanic rocks, much less is known as to the thermal properties of unlithified granular volcanic deposits. McCombie et al. (2017) found that the thermal conductivity of pozzolana from Rome (Italy) increased from ~0.2 to ~1.2 $W \cdot m^{-1} \cdot K^{-1}$ as the saturation degree increased from dry to fully saturated. The

thermal conductivity, thermal diffusivity, and specific heat capacity of dry unlithified volcanic deposits from the lava dome at La Soufrière de Guadeloupe (Eastern Caribbean) were measured to be 0.15−0.20 $W \cdot m^{-1} \cdot K^{-1}$, 0.17−0.24 $mm^2 \cdot s^{-1}$, and 0.68−1.04 $J \cdot kg^{-1} \cdot K^{-1}$, respectively (Heap et al., 2022a). The average dry and water-saturated thermal conductivity of volcanic soils from Hokkaido (Japan) was measured to be 0.14 and 0.52 $W \cdot m^{-1} \cdot K^{-1}$, respectively (Tarnawski et al., 2019). Finally, dry rhyolitic and basaltic ash from Kamchatka (Russia) was found to have a thermal conductivity of ~0.2 $W \cdot m^{-1} \cdot K^{-1}$, which increased to ~1.0−1.2 $W \cdot m^{-1} \cdot K^{-1}$ upon complete saturation with frozen water (Kuznetsova, 2017).

More thermal property data for unlithified granular volcanic materials, and a better understanding of factors that can influence these properties, can help improve models designed to interpret heat flux data and model heat loss from magma. In particular, there remains no constitutive material model that can be used to predict thermal properties of unlithified granular volcanic materials as a function of saturation degree, the state of particle packing, or the mineralogy and alteration. Here, therefore, we report findings from a laboratory study designed to better understand the thermal properties of unlithified granular volcanic materials, including the influence of hydrothermal alteration and degree of water saturation. Finally, we encapsulate our dataset in an empirical model framework (Johansen, 1975) for general use.

2 Materials and Methods

The materials used for this study were collected from La Soufrière de Guadeloupe, hereafter called La Soufrière, an active andesitic stratovolcano located on the French island of Guadeloupe in the Eastern Caribbean (Moretti et al., 2020; Figure 1). In total, 19 rock blocks were collected from different locations around the volcano (sampling locations are shown in Figure 1). These blocks have been previously used in recent studies focused on the influence of hydrothermal alteration on the compressive and tensile strength (Heap et al., 2021, 2022b, 2022c) and the thermal properties (Heap et al., 2022a) of volcanic rocks.

Of the 19 rock blocks collected, nine blocks were taken from the collapse scar of the 2009 landslide (H2A, H2B, H3, H4A, H5A, H6, H25, H29, and H30). Five blocks were collected from the dome summit: four blocks were taken from the lava spines of the 1530 CE dome (two blocks from Cratère Sud Central, H19 and H20, and two blocks from an adjacent site, H21 and H22), and one block was taken from the Lacroix Supérieur outgassing fracture (H18). We also collected blocks from the West wall of the fault “Faille 30 Août” (H14 and H15), the collapse scar of the landslide triggered by the 21 November 2004 Les Saintes magnitude Mw 6.3 regional earthquake (Feuillet et al., 2011) (WP1285), and from a lava adjacent to the Galion waterfall (H32). The final

block, a volcanic bomb from the 1976–1977 eruption, was taken from the roof of a small disused thermal bathhouse to the South of the dome (WP1317). These blocks are characterised by advanced argillic alteration, the result of the efficient circulation of acidic sulfate-chloride-rich fluids (below 350 °C, and down to 150–200 °C; pH < 4) (Heap et al., 2021).

Offcuts of each of the blocks were crushed and powdered by hand using a pestle and mortar. The powdered materials were then sieved to a grain diameter <1 mm and dried in a vacuum-oven at 40 °C for at least 48 h. The solid density of each powdered sample ρ_s was then measured using the mass and volume, measured by a helium pycnometer, of an aliquot of the oven-dry powder.

The thermal conductivity λ and thermal diffusivity D of the powders were measured using a Hot Disk® TPS 500 Thermal Constants Analyser using the transient plane source (TPS) method (Gustafsson, 1991; Harlé et al., 2019; Heap et al., 2020, 2022a). The TPS method uses a resistive sensor (the transient plane source) sandwiched between two samples to measure the increase in resistance as it heats the samples using an electrical current pulse. Because the geometry of the sensor is known, the average temperature increase as a function of time can be calculated, which can be then used to determine thermal conductivity and thermal diffusivity. The resistive sensor is therefore used as both the heat source and the temperature sensor.

Thermal conductivity and thermal diffusivity were measured using a sensor consisting of two 10 μm-thick nickel foil spirals (radius of 3.189 mm) that are encased and insulated by 30 μm-thick Kapton (Figure 2a). The powdered samples were measured using a sample holder of known volume supplied by Hot Disk®. The mass of the powder was first measured. Half of the powder was then spooned into the lower part of the sample holder. The powder in the sample holder was then manipulated using the spoon so that the surface of the powder was flat. The sample holder containing the powder was then placed underneath the sensor (Figure 2a). The top part of the sample holder was then placed on top of the lower part, and the remaining powder was spooned on top of the sensor and manipulated using the spoon to ensure a flat surface (Figure 2b). A metal plate was then placed on top of the sample assembly, and the entire sample assembly was compacted using a 3.5 kg weight (Figure 2c). The 3.5 kg weight ensured (1) a similar compaction from sample to sample (and therefore a similar porosity), (2) a good contact between the powder and the sensor, and (3) that the sensor was flat during the measurements. The bulk sample volume was calculated by measuring the height of the powder in the sample holder following compaction under a weight of 3.5 kg. The bulk sample density ρ_b was then calculated using the mass and volume of the powder. Finally, the total porosity of the powder ϕ_t was calculated using $\phi_t = 1 - (\rho_b/\rho_s)$.

Because temperature influences the measurements, the ambient room temperature adjacent to the sample, measured using a thermocouple, was inputted into the Thermal Constants Analyser prior to starting each measurement. In order to measure the thermal conductivity and thermal diffusivity of the samples, an electrical current of known power and for a fixed duration was passed through the sensor, which then recorded the increase in sample temperature as a function of time. The output power and test duration used were 70 mW and 20 s, respectively. Four consecutive measurements were performed on each powder, and we report herein the mean and standard error of these four measurements. Each measurement was performed at least five minutes apart to ensure that the sample had cooled back to the ambient temperature. The sensor measured the temperature drift of the sample for 40 seconds prior to each measurement to check whether the sample was in thermal equilibrium. If the sample temperature was not constant during this 40 second period, the data were not considered and the measurement was repeated. The specific heat capacity at constant pressure C_p of each sample was calculated using $C_p = \lambda/(\rho_b D)$. All measurements were conducted in a far-field environment that was at ambient laboratory temperature and pressure.

To provide an assessment of the precision of the Hot Disk® TPS 500 Thermal Constants Analyser, we measured the thermal conductivity and thermal diffusivity of the same pair of sandstone samples 100 times. The power and duration of each measurement was 180 mW and 5 s, respectively, and we waited at least 10 minutes between individual measurements. We used two discs, 40 mm in diameter and 20 mm in length, of Rothbach sandstone, a sandstone with a connected porosity of 0.2 and an average grain radius of 110 μm (Louis et al., 2007). The mineral composition of Rothbach sandstone is 68% quartz, 16% feldspar, 3% oxides and micas, and about 6% clays (Louis et al., 2007). The mean and standard error for the thermal conductivity are 2.878 and 0.007 $W \cdot m^{-1} \cdot K^{-1}$, respectively, and the mean and standard error for the thermal diffusivity are 1.884 and 0.027 $mm^2 \cdot s^{-1}$, respectively (all the data are provided in a Microsoft Excel spreadsheet that accompanies this contribution as Supplementary Material).

We additionally measured the thermal conductivity of the powders as a function of the degree of water saturation. The degree of water saturation S is defined here as the fraction of the porosity filled with water such that $S = \bar{V}_w/\phi_t$, where $\bar{V}_w$ is the volume ratio of water to sample. Therefore, S = 0 denotes a dry sample and S = 1 denotes a completely water-saturated sample with all of the porosity filled with water. We used the same Hot Disk® device described above, although the procedure differed in the following ways. Following the compaction of the dry powder under a weight of 3.5 kg, the weight and metal plate were removed and 5 ml of water was added to the sample using a syringe. The water was applied homogeneously throughout the top surface of the sample.

The metal plate and weight were placed back on the sample and we waited 10 min before starting the measurement to ensure that the water was evenly distributed throughout the sample (pilot experiments, in which we varied the volume of water and wait time and cut the partially-saturated powdered sample in half to visually inspect the cross section of the sample, suggested that 10 min was sufficient to ensure a uniform water distribution). The measurements were then performed as described above (output power and durations varied from 80–180 mW and 5–20 s, respectively). Once the measurements for a given saturation degree were complete, another aliquot of water was added (2–5 ml) and the procedure was continued until the sample was completely or almost-completely saturated.

The mineral phases present in each block was identified by a combination of optical microscopy, Raman spectroscopy, and X-ray powder diffraction (XRPD). Quantitative phase analysis was then performed using the XRPD data and the Rietveld approach. These data were previously published in (Heap et al., 2021, 2022a). The blocks contain primary plagioclase, pyroxene (clinopyroxene and orthopyroxene), and magnetite, and an alteration assemblage of secondary minerals consisting of variable quantities of kaolinite, alunite or natro-alunite, silica polymorphs (quartz, cristobalite, tridymite, and opal-A), hematite, pyrite, gypsum, and talc (Heap et al., 2021, 2022a). The alteration intensity of each block was quantified as the weight percentage (wt%) of secondary minerals (these values are provided in Table 1).

3 Results

3.1 Thermal properties of the dry volcanic powders

We first note that the total porosity of our powdered samples was essentially constant in the range 0.47–0.51 (Table 1), which speaks to the homogeneity of the powdered samples in terms of grainsizes, as well as the reproducibility of the packing-and-weight approach (Figure 2). Our data for the thermal conductivity, thermal diffusivity, and specific heat capacity for all the dry powdered samples are plotted as a function of alteration in Figure 3 (data available in Table 1). Figure 3a shows that thermal conductivity exhibits a modest decrease as a function of increasing alteration. Thermal conductivity decreases from ~0.3 $W \cdot m^{-1} \cdot K^{-1}$ at an alteration of ~10 wt% to ~0.2 $W \cdot m^{-1} \cdot K^{-1}$ at an alteration of ~70 wt% (Figure 3a). Figure 3b shows that thermal diffusivity also decreases as a function of increasing alteration. Thermal diffusivity decreases from ~0.27 $mm^2 \cdot s^{-1}$ at an alteration of ~10 wt% to ~0.22 $mm^2 \cdot s^{-1}$ at an alteration of ~70 wt% (Figure 3b). Specific heat capacity, however, does not appear to change systematically as a function of alteration (Figure 3c). Specific heat capacity varies between 0.6 and 0.9 $J \cdot kg^{-1} \cdot K^{-1}$ (Figure 3c).

209

210 3.2 Thermal conductivity as a function of water saturation degree

211 Thermal conductivity is plotted as a function of the degree of saturation with water in Figure 4 (data
212 available in Table 2). The colour of the symbols and lines on Figure 4 indicates the alteration, where red and yellow
213 indicate low and high alteration, respectively. Figure 4 shows that the thermal conductivity of the powders
214 increases as a non-linear function of saturation degree. In general, thermal conductivity increases from ~0.2–0.3
215 $W \cdot m^{-1} \cdot K^{-1}$ at a saturation degree of $S = 0$ up to ~0.8–1.1 $W \cdot m^{-1} \cdot K^{-1}$ at a saturation degree of $S \approx 0.7$, and remains
216 more-or-less constant up to the maximum saturation degree of $S = 1$ (Figure 4). This suggests that the effect of
217 increasing saturation degree is most pronounced at relatively low values of S, tailing off as the sample becomes
218 completely saturated (Figure 4).

219 Figure 4 also shows that the increase in thermal conductivity as a function of saturation degree appears
220 to depend on the alteration intensity. The increase in thermal conductivity per unit saturation is, in general, lower
221 for the highly altered samples (in yellow and orange) than for the relatively unaltered samples (in red) (Figure 4).
222 Further, the thermal conductivity at, or close to, complete saturation is lower as alteration increases (Figure 4).
223 Highly altered samples (in yellow and orange) have a thermal conductivity of ~0.8–1.0 $W \cdot m^{-1} \cdot K^{-1}$ at, or close to,
224 complete saturation, compared to ~1.0–1.2 $W \cdot m^{-1} \cdot K^{-1}$ for the relatively unaltered samples (in red) (Figure 4).

225

226 **4 Discussion**

227 4.1 Influence of alteration on the thermal properties of dry volcanic powders

228 Our data show that the thermal conductivity of dry unlithified volcanic material varies from ~0.2–0.3
229 $W \cdot m^{-1} \cdot K^{-1}$ (Table 1). These values are in broad agreement with previously published studies, who report thermal
230 conductivities for dry unlithified volcanic material of 0.15−0.20 $W \cdot m^{-1} \cdot K^{-1}$ (McCombie et al., 2017; Kuznetsova,
231 2017; Tarnawski et al., 2019; Heap et al., 2022a).

232 Our data also show that thermal conductivity and thermal diffusivity of volcanic powders decrease as a
233 function of alteration (Figure 3), in agreement with data collected for volcanic rock samples (Heap et al., 2022a).
234 Heap et al. (2022a) found, for rock samples prepared from the same blocks studied herein, that thermal
235 conductivity decreased from ~1.5 to ~0.6 $W \cdot m^{-1} \cdot K^{-1}$ as alteration increased from 6 to >70 wt%. However, these
236 data for volcanic rocks are also influenced by their varying porosities, another factor that is known to greatly
237 influence thermal conductivity (Robertson and Peck, 1974; Heap et al., 2020). Heap et al. (2022a) then used an
238 effective medium approach—the Maxwell equation (Zimmerman, 1989)—to estimate the thermal conductivity of

the solid groundmass (i.e., without porosity) λ_0 and found that λ_0 decreases as a function of alteration, from ~1.8 $W \cdot m^{-1} \cdot K^{-1}$ at an alteration of ~10 wt% to ~1.25 $W \cdot m^{-1} \cdot K^{-1}$ at an alteration of >70 wt%. The thermal property data measured here (Figure 3) are unaffected by the influence of porosity (since the porosities of the powders are essentially equal; Table 1) and therefore indicate that the thermal conductivity and thermal diffusivity of unlithified granular volcanic materials are indeed reduced as a result of increasing alteration. This can be explained by the lower thermal conductivity and thermal diffusivity of the alteration assemblage compared to the primary mineral assemblage. For example, the thermal conductivity of kaolinite, a common secondary mineral in the dome rocks from La Soufrière (Heap et al., 2021, 2022a), is lower that of plagioclase (Horai, 1971; Brigaud and Vasseur, 1989).

If we compare our values of thermal conductivity λ at a saturation degree of zero (i.e., $\lambda|_{S=0}$; the data shown in Figure 3a), hereafter termed λ_d, with the values for the solid groundmass λ_0 (from Heap et al., 2022a), we find that the degree to which the dry, but porous, conductivity of the powder λ_d depends on alteration is similar to the degree to which λ_0 depends on alteration (Figure 5a). The empirical linear regressions to the λ_d and λ_0 data as a function of alteration have very similar slopes (dashed lines on Figure 5a), albeit with different intercepts that reflect the porous vs. non-porous nature of λ_d and λ_0, respectively (Figure 5a). The covariance of λ_d and λ_0 is linear and an excellent fit ($r^2 = 0.987$) with an imposed intercept of 0 (dashed line on Figure 5b). This suggests that, at constant porosity, the thermal conductivity of the non-porous groundmass λ_0 is the first order control on the conductivity of the unlithified granular material λ_d at $S = 0$. This can be further confirmed by applying the geometric mean model $\lambda_d = \lambda_0^{1-\phi}\lambda_p^{\phi}$ (Judge, 1973), where λ_p is the conductivity of the pore fluid. In our case, $\lambda_p \approx 0.0367$ $W \cdot m^{-1} \cdot K^{-1}$ for air at the experimental temperature. When we use this value to predict λ_d as a function of λ_0 as described, and assuming $\phi = 0.47$, we find further good agreement with our data (solid line on Figure 5b).

4.2 Influence of water saturation degree and alteration on the thermal conductivity of volcanic powders

Our data show that thermal conductivity of volcanic powders increases as a function of the degree of water saturation (Figure 4). The thermal conductivity of rocks and unlithified granular materials has been previously seen to increase as a function of water saturation degree, and is due to the higher thermal conductivity of water compared to air (e.g., Clauser and Huenges, 1995; Coté and Konrad, 2005; Balland and Arp, 2005; Lu et al., 2007; Smits et al., 2010; Nagaraju and Roy, 2014; Barry-Macaulay et al., 2015; Zhang and Wang, 2017; Harlé et al., 2019; Heap et al., 2020). Our data are very much in agreement with the data provided by McCombie et al.

(2017) for pozzolana (pyroclastic soil) from Rome. These authors showed that thermal conductivity increased from ~0.2 to ~1.2 $W \cdot m^{-1} \cdot K^{-1}$ as the saturation degree increased from dry to fully saturated, very similar to the data presented herein (Figure 4).

To better understand our data, we use a model for the conductivity of variably saturated media (Johansen, 1975) that predicts that λ is linearly dependent on $\log_{10} S$ and is:

$$\lambda = \lambda_d + (\lambda_s - \lambda_d)(1 + \log_{10} S), \quad (1)$$

where λ_s is the conductivity of the fully saturated sample (i.e., $\lambda|_{S=1}$). Although various models exist to model the thermal conductivity of variably saturated media, we chose here the model of Johansen (1975) due to its widespread use in the study of soils and granular media (e.g., Coté and Konrad, 2005; Balland and Arp, 2005; Lu et al., 2007; Smits et al., 2010; Barry-Macaulay et al., 2015; Zhang and Wang, 2017). Equation (1) cannot be valid at low S because it predicts that $\lambda < 0$ W. m^{-1}. K^{-1} as $S \to 0$. For this reason, it is clearly valid only for moderate to high values of S. Specifically, λ will be greater than zero for $S > 10^{[\lambda_d/(\lambda_s - \lambda_d)]-1}$. Equation (1) can be rendered dimensionless, and therefore universal for all powder types (i.e., for all alteration values) by rearranging as:

$$\frac{\lambda - \lambda_d}{\lambda_s - \lambda_d} = 1 + \log_{10} S, \quad (2)$$

where we define the dimensionless conductivity as $\bar{\lambda} \equiv (\lambda - \lambda_d)/(\lambda_s - \lambda_d)$. This normalisation has the desirable property that at $\bar{\lambda} \to 0$, $\lambda \to \lambda_d$, and at $\bar{\lambda} \to 1$, $\lambda \to \lambda_s$ such that all of our data should be bounded $0 \leq \bar{\lambda} \leq 1$. In both Equations (1) and (2), λ_d is directly measured herein (see Figure 3a and Table 1). To find λ_s we can apply one of two approaches. First, we predict λ_s using the same approach as applied in Figure 5b for the dry case where the pore fluid is air: $\lambda_s = \lambda_0^{1-\phi}\lambda_p^{\phi}$. Here we simply exchange the value of λ_p that is valid for air, for the value valid for water λ_p = 0.599 $W \cdot m^{-1} \cdot K^{-1}$. This result is given in Figure 6a and, while it captures the general trend of the data, clearly the data are not bounded between 0 and 1 as expected, and the data $\bar{\lambda} > 1$ imply that λ_s may be incorrect (i.e. $\lambda_s = \lambda_0^{1-\phi}\lambda_p^{\phi}$ performs poorly with our saturated data at $S = 1$). Therefore, second, we can reduce the total dataset to just those samples for which λ was measured at $S = 1$ (samples H2B, H15, H21, and H30; see Table 2). These four samples cover a range of alteration from 41 to 74.6 wt% (Table 1). Now, when we use the measured λ_s values in Equation (2), we find excellent agreement between our data and the model without the need

for empirical adjustment or fitting (Figure 6b). In Figure 6b, it is clear that all data are well-bounded by $0 \leq \bar{\lambda} \leq 1$ as predicted. Using the data for these four samples, we can now specify the lower value of S below which Equation (1) or (2) is not valid. As stated, that lower limit is $S = 10^{[\lambda_d/(\lambda_s-\lambda_d)]-1}$, which is $S \approx 0.05$ according to the values of λ_d and λ_s that we measure (here taking approximately $\lambda_d = 0.25$ and λ_s = 1 W·m^{-1}·K^{-1}, respectively). Given the normalisation $\overline{\lambda}$, it is clear that while Equation (1) provides positive, and therefore sensible, values of λ for $S > 10^{[\lambda_s/(\lambda_d-\lambda_s)]}$, Equation (2) shows that the normalised values $\overline{\lambda}$ will only be positive for $S > 10^{-1}$ (i.e., $S >$ 0.1). This implies that in the region $0.05 \lesssim S \lesssim 0.1$, Equation (2) will predict positive λ values but at $\lambda < \lambda_d$.

The result given in Figure 6b suggests that across the range of alteration present in the four samples analysed (i.e., 41–74.6 wt%), there is no discernible effect of alteration on their thermal conductivity at different saturation degrees. This observation suggests that the dominant effect of alteration is captured in the end member values λ_d and λ_s, and can thus be deconvolved from the effect of saturation degree. Hence, by applying $\bar{\lambda}$, alteration does not enter into the saturation-conductivity model given by Equation (2).

In Figure 7 we show the dimensional data from Figure 6b along with the dimensional version of the model (i.e., Equation (1)). When compared with Figure 6a, it is clear that using the measured λ_d and λ_s far out-performs using the predicted λ_s value. The effect of alteration that is captured by these four datasets is limited compared with the apparent effect seen in Figure 4. And given the efficacy of the correlations in Figure 5, we anticipate that the dominant effect of alteration is in changing λ_d and λ_s. While the effect of alteration on λ_d is clearly attributable to the effect of alteration on the groundmass λ_0 (Figure 5), the effect of alteration on λ_s remains unexplained. This effect could also be related to λ_0. Although, we additionally hypothesise that the effect of alteration on λ_s could be the result of the higher wt% of kaolinite in the altered samples (Heap et al., 2021, 2022a), which can adsorb water (Croteau et al., 2009). Therefore, for the altered samples, some of the water may adsorb to the surface of mineral grains rather than residing within the void space, which may result in a lower λ_s.

4.3 Implications for the modelling of heat transport in a volcano or volcanic geothermal reservoir

Values for the thermal properties of volcanic rocks and unlithified granular volcanic materials are required in models designed to interpret surface heat flux data and model heat loss from magma. We provide three take-home points, based on the results of this study, to help those tasked with modelling heat transport within a volcano.

First, our study shows that, due to the potentially large difference in thermal properties between volcanic rocks and unlithified granular volcanic materials, it is important to know the proportions and/or locations of rock

328 and unlithified materials when modelling heat transport within a volcano. To emphasise, the thermal conductivity
329 of rocks from La Soufrière was measured to be ~0.5–1.5 $W \cdot m^{-1} \cdot K^{-1}$ (Heap et al., 2022a), whereas the thermal
330 conductivity of powders prepared from the same rocks was measured to be ~0.2–0.3 $W \cdot m^{-1} \cdot K^{-1}$ (Figure 3).

331 Second, our study shows that it is important to know the alteration state of the rocks and unlithified
332 materials. The thermal conductivity and thermal diffusivity of unlithified granular volcanic materials (Figure 3)
333 and volcanic rocks (Heap et al., 2022a) are reduced following hydrothermal alteration.

334 Finally, our study also shows that it is important to know the saturation degree of the rocks and unlithified
335 granular materials. This is especially important for the unlithified granular materials, which see larger increases in
336 thermal conductivity upon saturation (Figure 4) than rocks (Heap et al., 2020). Indeed, thermal conductivity values
337 for saturated powders can be similar to those for dry porous rocks (porosity > 0.2; Heap et al., 2022a) and even
338 some water-saturated porous rocks (porosity > 0.5; Heap et al., 2020) (Figure 8). The empirical model proposed
339 by Johansen (1975) for variably saturated granular media is in general agreement with our data, and provides a
340 means to model the thermal conductivity of unlithified granular volcanic materials as a function of saturation
341 degree (Figures 6 and 7). The importance of saturation degree on the thermal conductivity of volcanic rocks and
342 powders (Figure 8) suggests that geophysical methods able to map subsurface saturation, such as electrical
343 tomography (Rosas-Carbajal et al., 2016; Gresse et al., 2017; Byrdina et al., 2017; Ahmed et al., 2018; Ghorbani
344 et al., 2018), could be used to improve heat flux calculations and modelling designed to inform on volcanic and
345 geothermal processes.

346

347 **5 Conclusions**

348 The thermal properties of volcanic rocks and unlithified granular volcanic materials are required for
349 modelling and understanding surface heat fluxes at volcanoes, which can inform on growing volcanic unrest and
350 impending eruptive activity, and for models designed to estimate timescales for the cooling of magma. There are
351 comparatively few data for unlithified granular volcanic materials, however, which served as the motivation for
352 this contribution.

353 Our study has shown that the thermal properties of unlithified granular volcanic materials are low when
354 compared to rocks (~0.2–0.3 $W \cdot m^{-1} \cdot K^{-1}$ compared to ~0.5–1.5 $W \cdot m^{-1} \cdot K^{-1}$; Figure 3; Heap et al., 2022a) and that
355 they are influenced by alteration and saturation with water (Figures 3 and 4). We show that thermal conductivity
356 decreases from ~0.3 to ~0.2 $W \cdot m^{-1} \cdot K^{-1}$ and thermal diffusivity decreases from ~0.27 to ~0.22 $mm^2 \cdot s^{-1}$ as alteration
357 is increased from ~10 to ~70 wt% (Figures 3a and 3b). We interpret this to be the result of the lower thermal

conductivity and thermal diffusivity of the secondary mineral assemblage. Specific heat capacity, however, does not appear to change systematically as a function of alteration (Figure 3c).

We also show that thermal conductivity increases from ~0.2–0.3 to ~0.8–1.1 $W \cdot m^{-1} \cdot K^{-1}$ as the saturation degree is increased from dry to near-complete saturation (Figure 4), due to the higher thermal conductivity of water compared to air. We find that an empirical model for variably saturated granular media (Johansen, 1975) is in general agreement with our data (Figures 6 and 7), and provides a framework to predict the thermal conductivity of unlithified granular volcanic materials as a function of saturation degree. We also find that, when saturated, the thermal conductivity of altered unlithified materials is lower than that of unaltered unlithified materials (Figure 4). We interpret this latter point to be dominantly due to the effect of alteration on the groundmass conductivity (Figure 5), although we also suggest that this could also be due to the ability of kaolinite, abundant in the altered materials, to adsorb water. Finally, we show that saturated unlithified materials can have higher thermal conductivities than dry rocks (Figure 8), highlighting the importance of understanding the saturation state prior to performing heat flux calculations and modelling designed to inform on volcanic and geothermal processes.

It is our hope that the data and modelling presented in this study will assist those tasked with modelling heat transport within a volcano or volcanic geothermal reservoir. Improved models will help better assess volcanic hazards and mitigate risk and help optimise geothermal energy exploitation. Finally, we note that, although the blocks studied herein were collected to capture the breadth of alteration seen at La Soufrière, and so likely capture the range in expected thermal properties for La Soufrière, care should be taken to ensure that the type of alteration (advanced argillic alteration) is similar if these data are to be used for other volcanoes or volcanic systems. Because the thermal properties of unlithified granular volcanic materials depend on the thermal properties of the constituent minerals, the thermal properties of altered deposits with different secondary mineral assemblages may differ from those reported herein.

Acknowledgements

This work was supported by ANR grant MYGALE ("Modelling the phYsical and chemical Gradients of hydrothermal ALteration for warning systems of flank collapse at Explosive volcanoes"; ANR-21-CE49-0010). M. Heap also acknowledges support from the Institut Universitaire de France (IUF). We thank the IPGP for general funding for the Observatoires Volcanologiques et Sismologiques (OVS), INSU-CNRS for the funding provided by the Service National d'Observation en Volcanologie (SNOV), and the Ministère pour la Transition Ecologique (MTE) for financial support for the monitoring of the instable flank of La Soufrière de Guadeloupe. We thank

Marina Rosas-Carbajal, Jean-Christophe Komorowski, Patrick Baud, Lucille Carbillet, and Tomaso Esposti Ongaro for their help collecting the rocks used in this study. This study is LabEx ClerVolc contribution number 572. The constructive comments of two reviewers and the editor helped improve this manuscript.

Declaration of competing interest

The authors declare that they have no known competing financial interests or personal relationships that could have appeared to influence the work reported in this paper.

CRediT author statement

Michael Heap: Conceptualisation; Investigation; Resources; Writing – Original Draft; Visualisation; Project administration; Funding acquisition. **Fabian Wadsworth:** Formal analysis; Writing – Review & Editing. **David Jessop:** Writing – Review & Editing.

Supplementary Material

We provide a Microsoft Excel spreadsheet containing all the data collected for this study.

Figure 1. Map image of La Soufrière de Guadeloupe (Eastern Caribbean) showing the sample collection sites. Inset shows a map of Guadeloupe (with the location of the volcano given as a red triangle). Image data ©2019 Google.

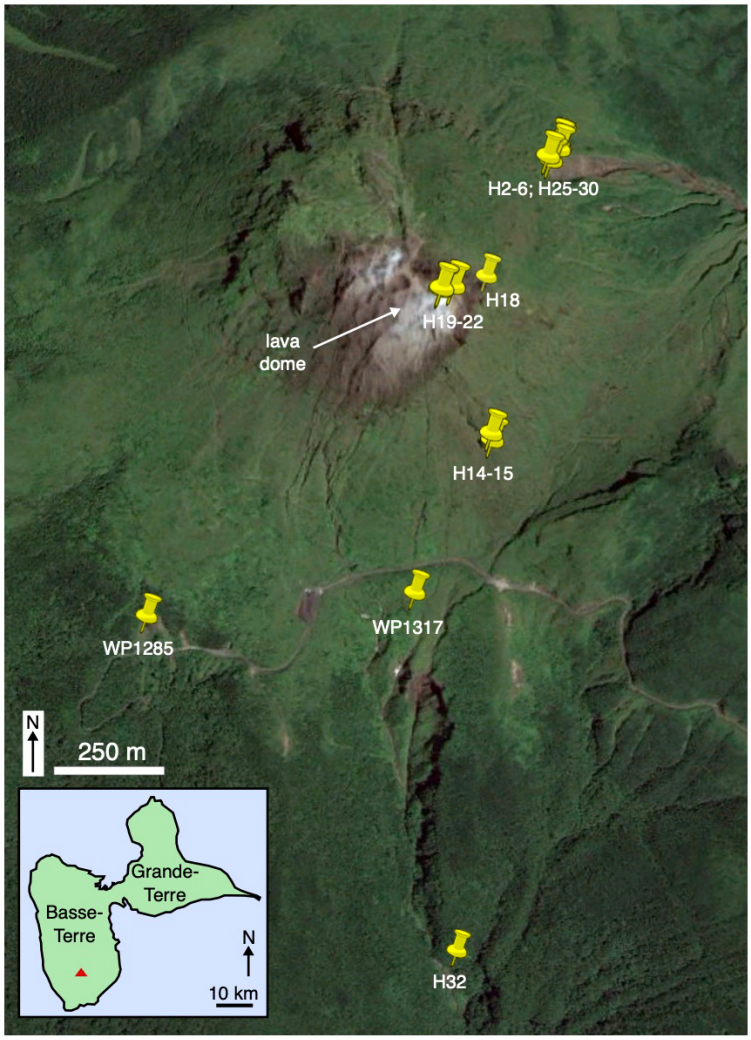

Figure 2. Photographs and a schematic diagram showing the procedure for measuring the powdered samples. (a) The powder was first spooned into the lower part of the holder, underneath the sensor. (b) The upper part of the holder was placed onto the lower part and powder was spooned over the sensor. (c) The top of the holder (a flat metal piece) was placed on top of the powder and a 3.5 kg weight was placed on top of the setup to ensure reproducible compaction (and therefore a similar porosity) and a good contact between the sensor and the powder. (d) Schematic (not-to-scale) diagrams showing a side-on view of the experimental steps shown in panels (a), (b), and (c).

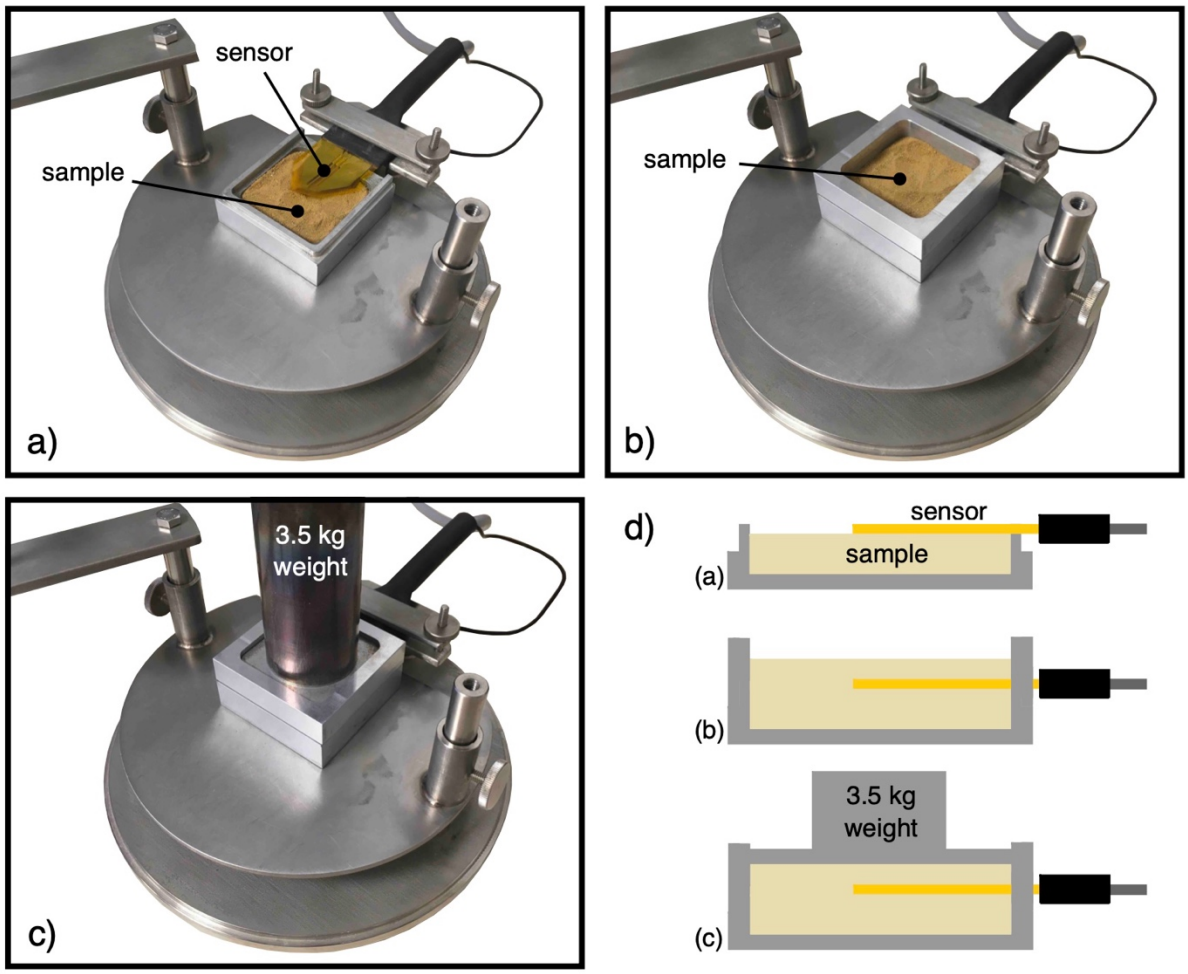

418 **Figure 3.** Thermal conductivity (a), thermal diffusivity (b), and specific heat capacity (c) as a function of alteration
419 (the wt% of secondary minerals) for dry powders from La Soufrière de Guadeloupe (Eastern Caribbean). Data
420 provided in Table 1.

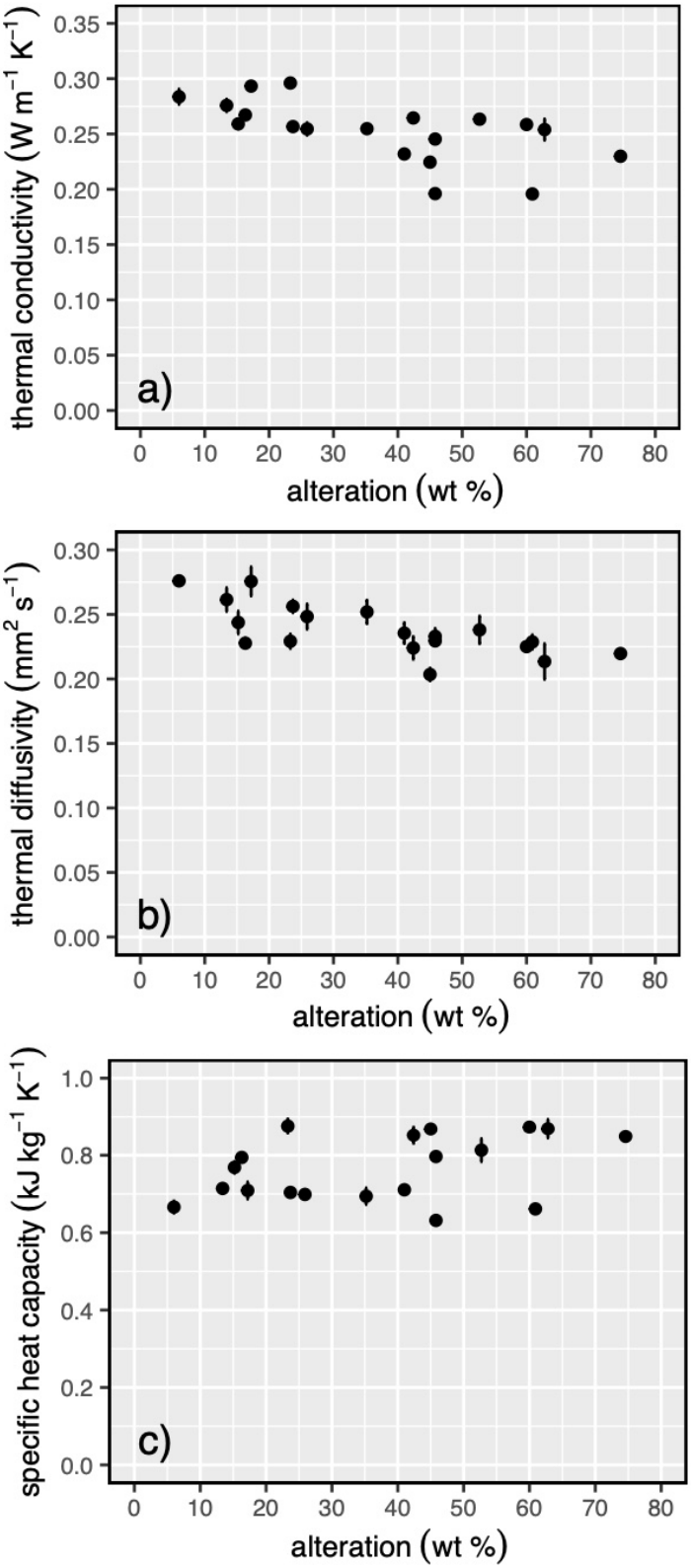

421

Figure 4. Thermal conductivity of powders from La Soufrière de Guadeloupe (Eastern Caribbean) as a function of water saturation degree S. Colour of the symbols and lines indicates the alteration (the wt% of secondary minerals), where red and yellow indicate low and high alteration, respectively.

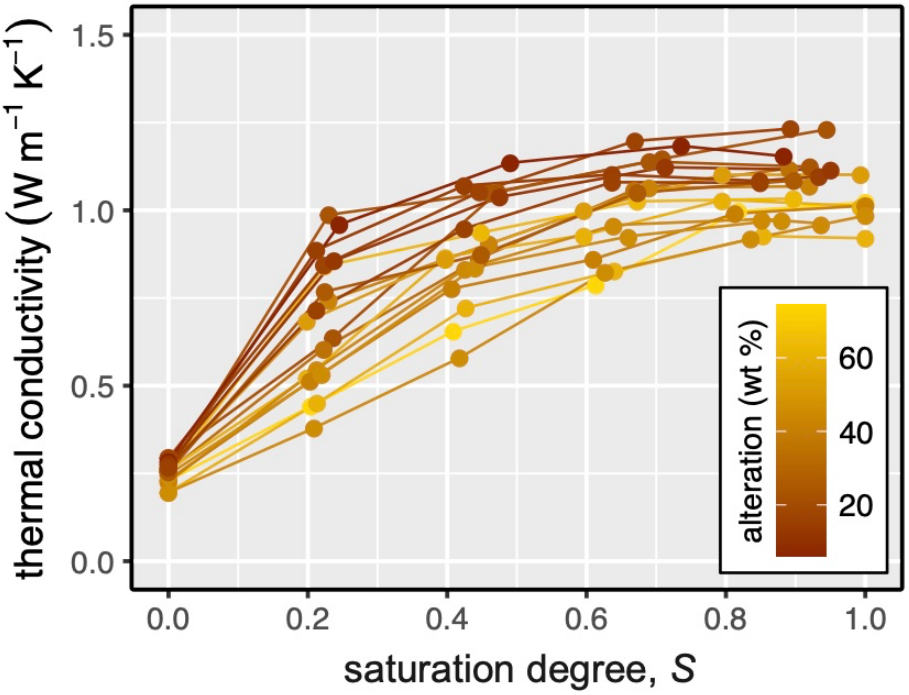

Figure 5. (a) The porosity-free groundmass conductivity λ_0 (red squares) and the conductivity of the dry powders at zero saturation ($S = 0$) λ_d (black circles) as a function of alteration (the wt% of secondary minerals). Dashed lines are empirical linear fits to the data. (b) The conductivity of the dry powders at zero saturation ($S = 0$) λ_d as a function of the porosity-free groundmass conductivity λ_0. The dashed line is an empirical linear fit to the data with an imposed intercept of 0. The solid curve is the theoretical trend following $\lambda_d = \lambda_0^{1-\phi}\lambda_p^{\phi}$ with $\lambda_p = 0.0367$ W·m^{-1}·K^{-1} and $\phi = 0.47$.

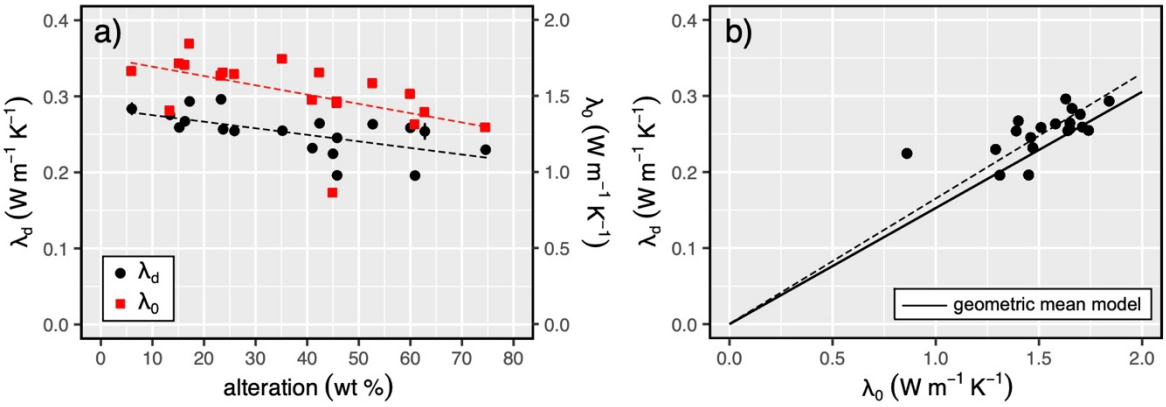

435 **Figure 6.** (a) Dimensionless conductivity, $\bar{\lambda} \equiv (\lambda - \lambda_d)/(\lambda_s - \lambda_d)$, as a function of saturation degree S for all the
436 data (Table 2). Black solid line is the modelled curve using Equation (2), in which the saturated conductivity is
437 predicted using $\lambda_s = \lambda_0^{1-\phi}\lambda_p^{\phi}$. (b) Dimensionless conductivity, $\bar{\lambda} \equiv (\lambda - \lambda_d)/(\lambda_s - \lambda_d)$, as a function of saturation
438 degree S for the data that reached complete saturation ($S = 1$; samples H2B, H15, H21, and H30). Black solid line
439 is the modelled curve using Equation (2), in which λ_s is measured directly (see Table 2). In both panels, the model
440 provides λ values valid above $S \approx 0.05$ (note that $\lambda \to 0$ occurs at $\bar{\lambda} < 0$ because $\lambda = 0$ is at $\lambda < \lambda_d$, which is why
441 the solid curves in this figure approach $\bar{\lambda} = 0$ at $S \approx 0.1$). Colour of the symbols indicates the alteration (the wt%
442 of secondary minerals), where red and yellow indicate low and high alteration, respectively.

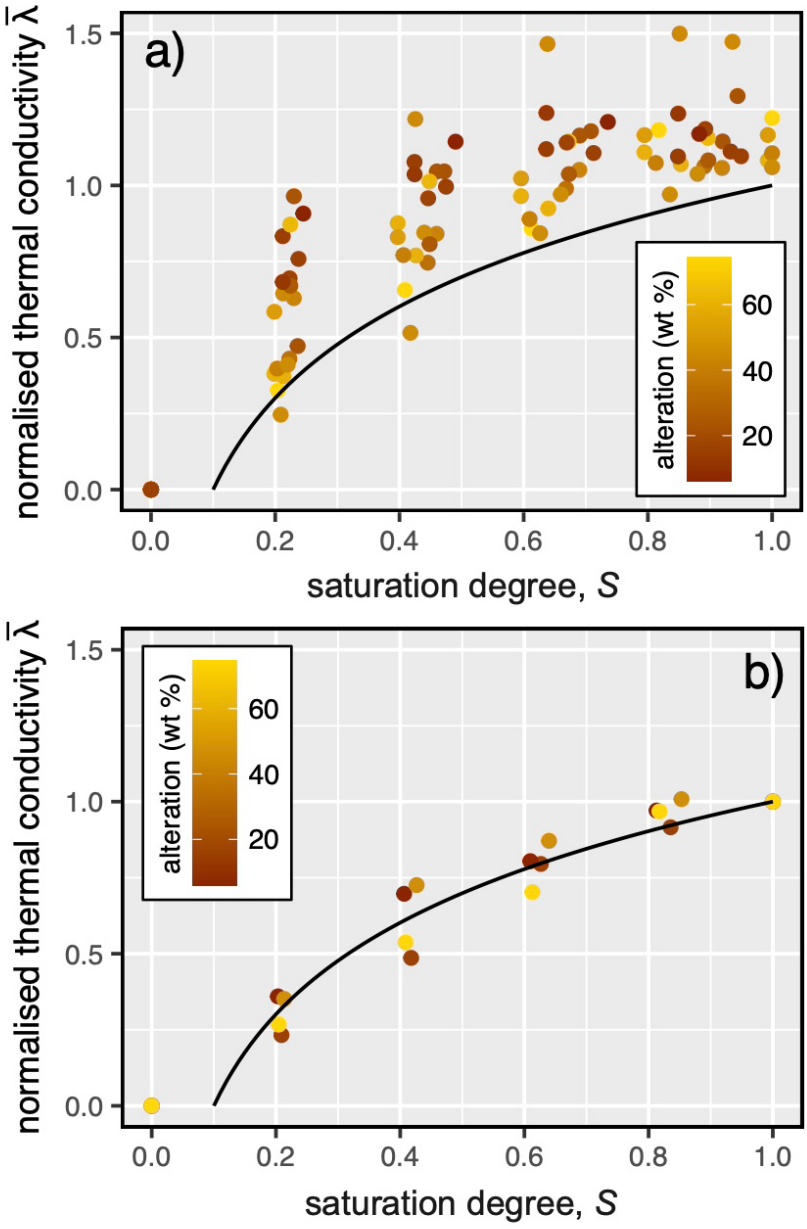

443

Figure 7. Dimensional thermal conductivity as a function of water saturation degree S for the four samples for which both the dry λ_d and saturated λ_s are measured values. The curves are given by Equation (1) with the measured values input (i.e., no fitting parameters). The model is valid above $S \approx 0.05$.

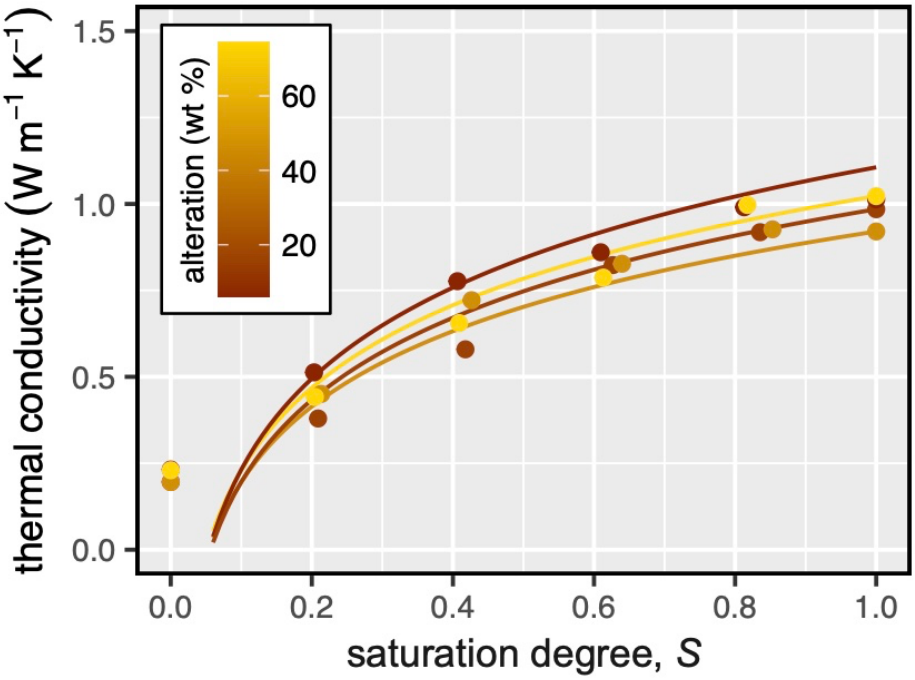

Figure 8. Thermal conductivity as a function of porosity for volcanic rocks (circles; data from Heap et al., 2020, 2022a) and unlithified granular volcanic materials (squares; data from Heap et al., 2022a and this study). Colour of the symbols indicates the water saturation degree, where light blue and dark blue indicate low and high saturation degree, respectively.

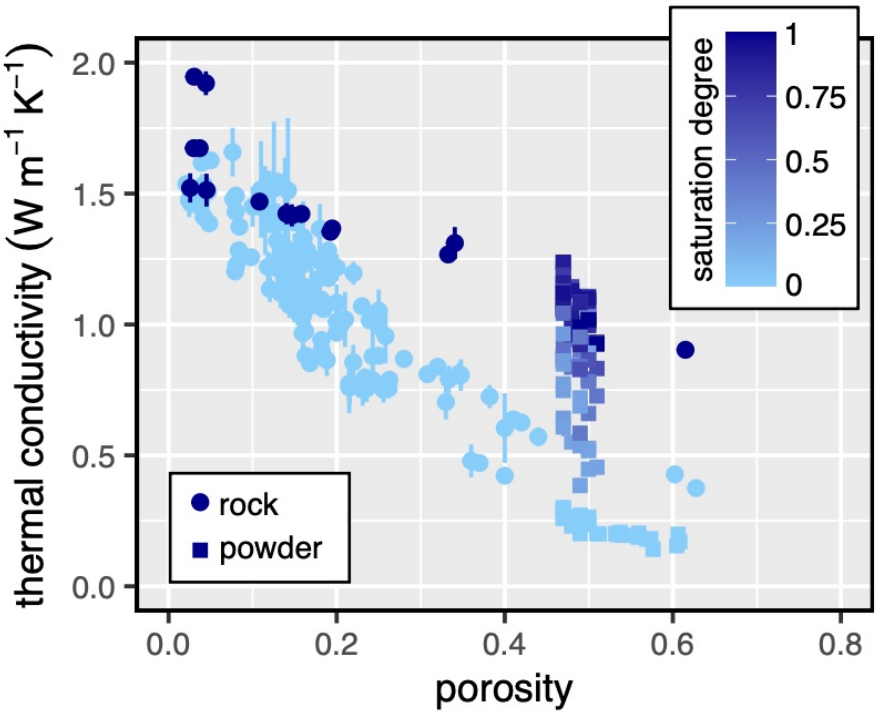

454 **Tables**

455

Block	Alteration (wt%)	Total porosity	Thermal conductivity [$W \cdot m^{-1} \cdot K^{-1}$]	Thermal diffusivity [$mm^2 \cdot s^{-1}$]	Specific heat capacity [$J \cdot kg^{-1} \cdot K^{-1}$]
H2A	23.3	0.47	0.296 ± 0.001	0.229 ± 0.006	0.876 ± 0.019
H2B	74.6	0.50	0.230 ± 0.001	0.220 ± 0.002	0.849 ± 0.007
H3	35.2	0.47	0.255 ± 0.001	0.252 ± 0.009	0.694 ± 0.021
H4A	60.0	0.50	0.259 ± 0.001	0.225 ± 0.003	0.873 ± 0.008
H5A	42.4	0.47	0.264 ± 0.004	0.224 ± 0.009	0.852 ± 0.021
H6	52.7	0.49	0.263 ± 0.003	0.238 ± 0.011	0.813 ± 0.029
H14	23.7	0.48	0.257 ± 0.002	0.256 ± 0.005	0.704 ± 0.008
H15	60.9	0.51	0.196 ± 0.002	0.229 ± 0.006	0.661 ± 0.008
H18	15.2	0.50	0.259 ± 0.004	0.244 ± 0.009	0.769 ± 0.015
H19	62.8	0.48	0.254 ± 0.010	0.214 ± 0.014	0.869 ± 0.024
H20	45.0	0.48	0.225 ± 0.003	0.203 ± 0.005	0.868 ± 0.009
H21	41.0	0.50	0.232 ± 0.004	0.236 ± 0.008	0.711 ± 0.012
H22	17.2	0.47	0.293 ± 0.004	0.276 ± 0.011	0.709 ± 0.022
H25	45.8	0.49	0.245 ± 0.002	0.230 ± 0.003	0.797 ± 0.009
H29	25.9	0.47	0.255 ± 0.006	0.248 ± 0.010	0.699 ± 0.012
H30	45.8	0.49	0.196 ± 0.003	0.233 ± 0.006	0.632 ± 0.008
H32	6.0	0.47	0.284 ± 0.007	0.276 ± 0.002	0.666 ± 0.016
WP1285	13.4	0.47	0.276 ± 0.006	0.261 ± 0.009	0.714 ± 0.011
WP1317	16.3	0.49	0.267 ± 0.001	0.228 ± 0.004	0.794 ± 0.012

456

457 **Table 1.** Thermal properties (thermal conductivity, thermal diffusivity, and specific heat capacity) of the 19 dry
458 powders from La Soufrière de Guadeloupe (Eastern Caribbean). Also provided are their alteration intensities (the
459 wt% of secondary minerals) and their total porosities. The thermal properties of each sample were measured four
460 times and we report the mean and standard error of these four measurements (all the data are provided in a
461 Microsoft Excel spreadsheet that accompanies this contribution as Supplementary Material).

462

Block	Alteration (wt%)	Total porosity	Saturation degree, S	Thermal conductivity [$W \cdot m^{-1} \cdot K^{-1}$]
H2A	23.3	0.47	0.00	0.296 ± 0.001
H2A	23.3	0.47	0.24	0.637 ± 0.018
H2A	23.3	0.47	0.47	1.052 ± 0.002
H2A	23.3	0.47	0.71	1.147 ± 0.011
H2A	23.3	0.47	0.94	1.231 ± 0.005
H2B	74.6	0.50	0.00	0.230 ± 0.001
H2B	74.6	0.50	0.20	0.442 ± 0.005
H2B	74.6	0.50	0.41	0.655 ± 0.005
H2B	74.6	0.50	0.61	0.787 ± 0.005

H2B	74.6	0.50	0.82	0.997 ± 0.006
H2B	74.6	0.50	1.00	1.023 ± 0.014
H3	35.2	0.47	0.00	0.255 ± 0.001
H3	35.2	0.47	0.22	0.604 ± 0.036
H3	35.2	0.47	0.45	0.860 ± 0.006
H3	35.2	0.47	0.67	1.057 ± 0.003
H3	35.2	0.47	0.89	1.116 ± 0.003
H4A	60.0	0.50	0.00	0.259 ± 0.001
H4A	60.0	0.50	0.20	0.522 ± 0.004
H4A	60.0	0.50	0.40	0.865 ± 0.005
H4A	60.0	0.50	0.60	0.927 ± 0.006
H4A	60.0	0.50	0.79	1.027 ± 0.002
H4A	60.0	0.50	0.99	1.008 ± 0.011
H5A	42.4	0.47	0.00	0.264 ± 0.004
H5A	42.4	0.47	0.23	0.743 ± 0.009
H5A	42.4	0.47	0.46	0.904 ± 0.007
H5A	42.4	0.47	0.69	1.064 ± 0.008
H5A	42.4	0.47	0.92	1.069 ± 0.011
H6	52.7	0.49	0.00	0.263 ± 0.003
H6	52.7	0.49	0.20	0.684 ± 0.007
H6	52.7	0.49	0.40	0.860 ± 0.028
H6	52.7	0.49	0.60	0.999 ± 0.018
H6	52.7	0.49	0.79	1.101 ± 0.008
H6	52.7	0.49	0.99	1.102 ± 0.005
H14	23.7	0.48	0.00	0.257 ± 0.002
H14	23.7	0.48	0.23	0.987 ± 0.014
H14	23.7	0.48	0.46	1.049 ± 0.009
H14	23.7	0.48	0.69	1.139 ± 0.019
H14	23.7	0.48	0.92	1.124 ± 0.005
H15	60.9	0.51	0.00	0.196 ± 0.002
H15	60.9	0.51	0.21	0.450 ± 0.004
H15	60.9	0.51	0.43	0.722 ± 0.018
H15	60.9	0.51	0.64	0.827 ± 0.014
H15	60.9	0.51	0.85	0.927 ± 0.022
H15	60.9	0.51	1.00	0.920 ± 0.015
H18	15.2	0.50	0.00	0.259 ± 0.004
H18	15.2	0.50	0.21	0.886 ± 0.008
H18	15.2	0.50	0.42	1.070 ± 0.017
H18	15.2	0.50	0.64	1.102 ± 0.017
H18	15.2	0.50	0.85	1.084 ± 0.009
H18	15.2	0.50	0.93	1.096 ± 0.002
H19	62.8	0.48	0.00	0.254 ± 0.010
H19	62.8	0.48	0.22	0.841 ± 0.013
H19	62.8	0.48	0.45	0.937 ± 0.019
H19	62.8	0.48	0.67	1.026 ± 0.012
H19	62.8	0.48	0.90	1.033 ± 0.009
H20	45.0	0.48	0.00	0.225 ± 0.003

H20	45.0	0.48	0.21	0.546 ± 0.017
H20	45.0	0.48	0.43	0.832 ± 0.010
H20	45.0	0.48	0.64	0.955 ± 0.011
H20	45.0	0.48	0.85	0.972 ± 0.005
H20	45.0	0.48	0.94	0.958 ± 0.012
H21	41.0	0.50	0.00	0.232 ± 0.004
H21	41.0	0.50	0.20	0.513 ± 0.008
H21	41.0	0.50	0.41	0.777 ± 0.010
H21	41.0	0.50	0.61	0.860 ± 0.028
H21	41.0	0.50	0.81	0.991 ± 0.025
H21	41.0	0.50	1.00	1.013 ± 0.007
H22	17.2	0.47	0.00	0.293 ± 0.004
H22	17.2	0.47	0.22	0.844 ± 0.007
H22	17.2	0.47	0.45	1.052 ± 0.006
H22	17.2	0.47	0.67	1.198 ± 0.021
H22	17.2	0.47	0.89	1.233 ± 0.004
H25	45.8	0.49	0.00	0.245 ± 0.002
H25	45.8	0.49	0.22	0.532 ± 0.002
H25	45.8	0.49	0.44	0.835 ± 0.005
H25	45.8	0.49	0.66	0.923 ± 0.015
H25	45.8	0.49	0.88	0.970 ± 0.006
H29	25.9	0.47	0.00	0.255 ± 0.006
H29	25.9	0.47	0.22	0.768 ± 0.004
H29	25.9	0.47	0.45	0.874 ± 0.015
H29	25.9	0.47	0.67	1.050 ± 0.026
H29	25.9	0.47	0.90	1.085 ± 0.014
H30	45.8	0.49	0.00	0.196 ± 0.003
H30	45.8	0.49	0.21	0.380 ± 0.021
H30	45.8	0.49	0.42	0.580 ± 0.020
H30	45.8	0.49	0.63	0.823 ± 0.002
H30	45.8	0.49	0.84	0.918 ± 0.004
H30	45.8	0.49	1.00	0.985 ± 0.030
H32	6.0	0.47	0.00	0.284 ± 0.007
H32	6.0	0.47	0.25	0.959 ± 0.011
H32	6.0	0.47	0.49	1.135 ± 0.010
H32	6.0	0.47	0.74	1.184 ± 0.007
H32	6.0	0.47	0.88	1.154 ± 0.001
WP1285	13.4	0.47	0.00	0.276 ± 0.006
WP1285	13.4	0.47	0.24	0.856 ± 0.012
WP1285	13.4	0.47	0.48	1.038 ± 0.011
WP1285	13.4	0.47	0.71	1.123 ± 0.020
WP1285	13.4	0.47	0.95	1.115 ± 0.012
WP1317	16.3	0.49	0.00	0.267 ± 0.001
WP1317	16.3	0.49	0.21	0.715 ± 0.011
WP1317	16.3	0.49	0.42	0.947 ± 0.011
WP1317	16.3	0.49	0.64	1.080 ± 0.006
WP1317	16.3	0.49	0.85	1.079 ± 0.006

463

Table 2. Thermal conductivity of the 19 powders from La Soufrière de Guadeloupe (Eastern Caribbean) at different degrees of water saturation. Also provided are their alteration intensities (the wt% of secondary minerals) and their total porosities. The thermal properties of each sample were measured four times and we report the mean and standard error of these four measurements (all the data are provided in a Microsoft Excel spreadsheet that accompanies this contribution as Supplementary Material).

References

Ahmed, A. S., Revil, A., Byrdina, S., Coperey, A., Gailler, L., Grobbe, N., ... & Humaida, H. (2018). 3D electrical conductivity tomography of volcanoes. Journal of Volcanology and Geothermal Research, 356, 243-263.

Annen, C., Pichavant, M., Bachmann, O., & Burgisser, A. (2008). Conditions for the growth of a long-lived shallow crustal magma chamber below Mount Pelee volcano (Martinique, Lesser Antilles Arc). Journal of Geophysical Research: Solid Earth, 113(B7).

Annen, C. (2017). Factors affecting the thickness of thermal aureoles. Frontiers in Earth Science, 5, 82.

Bagdassarov, N., & Dingwell, D. (1994). Thermal properties of vesicular rhyolite. Journal of Volcanology and Geothermal Research, 60(2), 179-191.

Balland, V., & Arp, P. A. (2005). Modeling soil thermal conductivities over a wide range of conditions. Journal of Environmental Engineering and Science, 4(6), 549-558.

Barry-Macaulay, D., Bouazza, A., Wang, B., & Singh, R. M. (2015). Evaluation of soil thermal conductivity models. Canadian Geotechnical Journal, 52(11), 1892-1900.

Bloomberg, S., Werner, C., Rissmann, C., Mazot, A., Horton, T., Gravley, D., ... & Oze, C. (2014). Soil CO 2 emissions as a proxy for heat and mass flow assessment, T aupō V olcanic Z one, N ew Z ealand. Geochemistry, Geophysics, Geosystems, 15(12), 4885-4904.

Branney, M. J., Kokelaar, P., & Kokelaar, B. P. (2002). Pyroclastic density currents and the sedimentation of ignimbrites. Geological Society of London. Vol. 27. https://doi.org/10.1144/GSL.MEM.2003.027.

Brigaud, F., & Vasseur, G. (1989). Mineralogy, porosity and fluid control on thermal conductivity of sedimentary rocks. Geophysical Journal International, 98(3), 525-542.

Brown, R. J., & Andrews, G. D. (2015). Deposits of pyroclastic density currents. In The encyclopedia of volcanoes (pp. 631-648). Academic Press.

Bruce, P. M., & Huppert, H. E. (1989). Thermal control of basaltic fissure eruptions. Nature, 342(6250), 665-667.

Byrdina, S., Friedel, S., Vandemeulebrouck, J., Budi-Santoso, A., Suryanto, W., Rizal, M. H., & Winata, E. (2017). Geophysical image of the hydrothermal system of Merapi volcano. Journal of Volcanology and Geothermal Research, 329, 30-40.

Carrigan, C. R. (1984). Time and temperature dependent convection models of cooling reservoirs: Application to volcanic sills. Geophysical Research Letters, 11(8), 693-696.

Carrigan, C. R., Schubert, G., & Eichelberger, J. C. (1992). Thermal and dynamical regimes of single-and two-phase magmatic flow in dikes. Journal of Geophysical Research: Solid Earth, 97(B12), 17377-17392.

Chiodini, G., Granieri, D., Avino, R., Caliro, S., Costa, A., & Werner, C. (2005). Carbon dioxide diffuse degassing and estimation of heat release from volcanic and hydrothermal systems. Journal of Geophysical Research: Solid Earth, 110(B8).

Chiodini, G., Cardellini, C., Lamberti, M. C., Agusto, M., Caselli, A., Liccioli, C., ... & Caliro, S. (2015). Carbon dioxide diffuse emission and thermal energy release from hydrothermal systems at Copahue–Caviahue Volcanic Complex (Argentina). Journal of Volcanology and Geothermal Research, 304, 294-303.

Clauser, C., & Huenges, E. (1995). Thermal conductivity of rocks and minerals. Rock physics and phase relations: a handbook of physical constants, 3, 105-126.

Côté, J., & Konrad, J. M. (2005). A generalized thermal conductivity model for soils and construction materials. Canadian Geotechnical Journal, 42(2), 443-458.

Dehn, J., Dean, K., & Engle, K. (2000). Thermal monitoring of North Pacific volcanoes from space. Geology, 28(8), 755-758.

Dufek, J., Ongaro, T. E., & Roche, O. (2015). Pyroclastic density currents: processes and models. In The encyclopedia of volcanoes (pp. 617-629). Academic Press.

Feuillet, N., Beauducel, F., & Tapponnier, P. (2011). Tectonic context of moderate to large historical earthquakes in the Lesser Antilles and mechanical coupling with volcanoes. Journal of Geophysical Research: Solid Earth, 116(B10).

Fialko, Y. A., & Rubin, A. M. (1999). Thermal and mechanical aspects of magma emplacement in giant dike swarms. Journal of Geophysical Research: Solid Earth, 104(B10), 23033-23049.
Fujii, N., & Osako, M. (1973). Thermal diffusivity of lunar rocks under atmospheric and vacuum conditions. Earth and Planetary Science Letters, 18(1), 65-71.
Ghorbani, A., Revil, A., Coperey, A., Ahmed, A. S., Roque, S., Heap, M. J., ... & Viveiros, F. (2018). Complex conductivity of volcanic rocks and the geophysical mapping of alteration in volcanoes. Journal of Volcanology and Geothermal Research, 357, 106-127.
Girona, T., Realmuto, V., & Lundgren, P. (2021). Large-scale thermal unrest of volcanoes for years prior to eruption. Nature Geoscience, 14(4), 238-241.
Goto, Y., Nakada, S., Kurokawa, M., Shimano, T., Sugimoto, T., Sakuma, S., ... & Uto, K. (2008). Character and origin of lithofacies in the conduit of Unzen volcano, Japan. Journal of volcanology and geothermal research, 175(1-2), 45-59.
Gresse, M., Vandemeulebrouck, J., Byrdina, S., Chiodini, G., Revil, A., Johnson, T. C., ... & Metral, L. (2017). Three-dimensional electrical resistivity tomography of the Solfatara crater (Italy): Implication for the multiphase flow structure of the shallow hydrothermal system. Journal of Geophysical Research: Solid Earth, 122(11), 8749-8768.
Gustafsson, S. E. (1991). Transient plane source techniques for thermal conductivity and thermal diffusivity measurements of solid materials. Review of scientific instruments, 62(3), 797-804.
Harlé, P., Kushnir, A. R., Aichholzer, C., Heap, M. J., Hehn, R., Maurer, V., ... & Duringer, P. (2019). Heat flow density estimates in the Upper Rhine Graben using laboratory measurements of thermal conductivity on sedimentary rocks. Geothermal Energy, 7(1), 1-36.
Harris, A. J., Blake, S., Rothery, D. A., & Stevens, N. F. (1997). A chronology of the 1991 to 1993 Mount Etna eruption using advanced very high resolution radiometer data: Implications for real-time thermal volcano monitoring. Journal of Geophysical Research: Solid Earth, 102(B4), 7985-8003.
Harris, A. J. L., Pilger, E., Flynn, L. P., Garbeil, H., Mouginis-Mark, P. J., Kauahikaua, J., & Thornber, C. (2001). Automated, high temporal resolution, thermal analysis of Kilauea volcano, Hawai'i, using GOES satellite data. International Journal of Remote Sensing, 22(6), 945-967.
Heap, M. J., Violay, M., Wadsworth, F. B., & Vasseur, J. (2017). From rock to magma and back again: the evolution of temperature and deformation mechanism in conduit margin zones. Earth and Planetary Science Letters, 463, 92-100.
Heap, M. J., Kushnir, A. R., Vasseur, J., Wadsworth, F. B., Harlé, P., Baud, P., ... & Deegan, F. M. (2020). The thermal properties of porous andesite. Journal of Volcanology and Geothermal Research, 398, 106901.
Heap, M. J., Baumann, T. S., Rosas-Carbajal, M., Komorowski, J. C., Gilg, H. A., Villeneuve, M., ... & Reuschlé, T. (2021). Alteration-Induced Volcano Instability at La Soufrière de Guadeloupe (Eastern Caribbean). Journal of Geophysical Research: Solid Earth, 126(8), e2021JB022514.
Heap, M. J., Jessop, D. E., Wadsworth, F. B., Rosas-Carbajal, M., Komorowski, J. C., Gilg, H. A., ... & Moretti, R. (2022a). The thermal properties of hydrothermally altered andesites from La Soufrière de Guadeloupe (Eastern Caribbean). Journal of Volcanology and Geothermal Research, 421, 107444.
Heap, M. J., Harnett, C. E., Wadsworth, F. B., Gilg, H. A., Carbillet, L., Rosas-Carbajal, M., ... & Moretti, R. (2022b). The tensile strength of hydrothermally altered volcanic rocks. Journal of Volcanology and Geothermal Research, 107576.
Heap, M. J., Troll, V. R., Harris, C., Gilg, H. A., Moretti, R., Rosas-Carbajal, M., ... & Baud, P. (2022c). Whole-rock oxygen isotope ratios as a proxy for the strength and stiffness of hydrothermally altered volcanic rocks. Bulletin of Volcanology, 84(8), 1-14.
Heiken, G., & Wohletz, K. (1991). Fragmentation processes in explosive volcanic eruptions. In: Sedimentation in Volcanic Settings (Eds: R.V. Fisher and G.A. Smith). SEPM Special Publication Number 45. https://doi.org/10.2110/pec.91.45.0019.
Hofmeister, A. (2019). Heat Transport and Energetics of the Earth and Rocky Planets. Elsevier. https://doi.org/10.1016/C2018-0-04206-1.
Horai, K., Simmons, G., Kanamori, H., & Wones, D. (1970). Thermal diffusivity, conductivity and thermal inertia of Apollo 11 lunar material. Geochimica et Cosmochimica Acta Supplement, 1, 2243.
Horai, K. I. (1971). Thermal conductivity of rock-forming minerals. Journal of geophysical research, 76(5), 1278-1308.
Irvine, T. N. (1970). Heat transfer during solidification of layered intrusions. I. Sheets and sills. Canadian Journal of Earth Sciences, 7(4), 1031-1061.
Jessop, D. E., Moune, S., Moretti, R., Gibert, D., Komorowski, J. C., Robert, V., ... & Burtin, A. (2021). A multi-decadal view of the heat and mass budget of a volcano in unrest: La Soufrière de Guadeloupe (French West Indies). Bulletin of Volcanology, 83(3), 1-19.
Johansen, O. (1975). Thermal conductivity of soils. Ph. D thesis. University of Trondheim (Norway).

Judge, A. S. (1973). The thermal regime of the Mackenzie Valley: observations of the natural state. Environmental-Social Committee, Northern Pipelines, Task Force on Northern Oil Development.
Kennedy, B. M., Farquhar, A., Hilderman, R., Villeneuve, M. C., Heap, M. J., Mordensky, S., ... & Reuschlé, T. (2020). Pressure controlled permeability in a conduit filled with fractured hydrothermal breccia reconstructed from ballistics from Whakaari (White Island), New Zealand. Geosciences, 10(4), 138.
Kolzenburg, S., & Russell, J. K. (2014). Welding of pyroclastic conduit infill: A mechanism for cyclical explosive eruptions. Journal of Geophysical Research: Solid Earth, 119(7), 5305-5323.
Kueppers, U., Scheu, B., Spieler, O., & Dingwell, D. B. (2006). Fragmentation efficiency of explosive volcanic eruptions: A study of experimentally generated pyroclasts. Journal of Volcanology and Geothermal Research, 153(1-2), 125-135.
Kuznetsova, E. (2017). Thermal conductivity and the unfrozen water contents of volcanic ash deposits in cold climate conditions: A review. Clays and Clay Minerals, 65(3), 168-183.
Louis, L., Wong, T. F., & Baud, P. (2007). Imaging strain localization by X-ray radiography and digital image correlation: Deformation bands in Rothbach sandstone. Journal of Structural Geology, 29(1), 129-140.
Lu, S., Ren, T., Gong, Y., & Horton, R. (2007). An improved model for predicting soil thermal conductivity from water content at room temperature. Soil Science Society of America Journal, 71(1), 8-14.
Mannini, S., Harris, A. J., Jessop, D. E., Chevrel, M. O., & Ramsey, M. S. (2019). Combining Ground-and ASTER-Based Thermal Measurements to Constrain Fumarole Field Heat Budgets: The Case of Vulcano Fossa 2000–2019. Geophysical Research Letters, 46(21), 11868-11877.
Mattsson, T., Burchardt, S., Almqvist, B. S., & Ronchin, E. (2018). Syn-emplacement fracturing in the Sandfell laccolith, eastern Iceland—Implications for rhyolite intrusion growth and volcanic hazards. Frontiers in Earth Science, 6, 5.
McCombie, M. L., Tarnawski, V. R., Bovesecchi, G., Coppa, P., & Leong, W. H. (2017). Thermal conductivity of pyroclastic soil (Pozzolana) from the environs of Rome. International Journal of Thermophysics, 38(2), 1-15.
Mielke, P., Nehler, M., Bignall, G., & Sass, I. (2015). Thermo-physical rock properties and the impact of advancing hydrothermal alteration—A case study from the Tauhara geothermal field, New Zealand. Journal of Volcanology and Geothermal Research, 301, 14-28.
Mielke, P., Weinert, S., Bignall, G., & Sass, I. (2016). Thermo-physical rock properties of greywacke basement rock and intrusive lavas from the Taupo Volcanic Zone, New Zealand. Journal of Volcanology and Geothermal Research, 324, 179-189.
Mielke, P., Bär, K., & Sass, I. (2017). Determining the relationship of thermal conductivity and compressional wave velocity of common rock types as a basis for reservoir characterization. Journal of Applied Geophysics, 140, 135-144.
Moretti, R., Komorowski, J. C., Ucciani, G., Moune, S., Jessop, D., de Chabalier, J. B., ... & Chaussidon, M. (2020). The 2018 unrest phase at La Soufrière of Guadeloupe (French West Indies) andesitic volcano: Scrutiny of a failed but prodromal phreatic eruption. Journal of Volcanology and Geothermal Research, 393, 106769.
Nabelek, P. I., Hofmeister, A. M., & Whittington, A. G. (2012). The influence of temperature-dependent thermal diffusivity on the conductive cooling rates of plutons and temperature-time paths in contact aureoles. Earth and Planetary Science Letters, 317, 157-164.
Nagaraju, P., & Roy, S. (2014). Effect of water saturation on rock thermal conductivity measurements. Tectonophysics, 626, 137-143.
Norton, D., & Knight, J. (1977). Transport phenomena in hydrothermal systems: cooling plutons. Am. J. Sci.;(United States), 277.
Pyle, D. M. (1989). The thickness, volume and grainsize of tephra fall deposits. Bulletin of Volcanology, 51(1), 1-15.
Robertson, E. C., & Peck, D. L. (1974). Thermal conductivity of vesicular basalt from Hawaii. Journal of Geophysical Research, 79(32), 4875-4888.
Romine, W. L., Whittington, A. G., Nabelek, P. I., & Hofmeister, A. M. (2012). Thermal diffusivity of rhyolitic glasses and melts: effects of temperature, crystals and dissolved water. Bulletin of volcanology, 74(10), 2273-2287.
Rosas-Carbajal, M., Komorowski, J. C., Nicollin, F., & Gibert, D. (2016). Volcano electrical tomography unveils edifice collapse hazard linked to hydrothermal system structure and dynamics. Scientific Reports, 6(1), 1-11.
Rust, A. C., Cashman, K. V., & Wallace, P. J. (2004). Magma degassing buffered by vapor flow through brecciated conduit margins. Geology, 32(4), 349-352.
Smits, K. M., Sakaki, T., Limsuwat, A., & Illangasekare, T. H. (2010). Thermal conductivity of sands under varying moisture and porosity in drainage–wetting cycles. Vadose Zone Journal, 9(1), 172-180.

635 Stevenson, J. A., & Varley, N. (2008). Fumarole monitoring with a handheld infrared camera: Volcán de Colima,
636 Mexico, 2006–2007. Journal of Volcanology and Geothermal Research, 177(4), 911-924.
637 Tarnawski, V. R., Tsuchiya, F., Coppa, P., & Bovesecchi, G. (2019). Volcanic soils: inverse modeling of thermal
638 conductivity data. International Journal of Thermophysics, 40(2), 1-25.
639 Tsang, S. W., Lindsay, J. M., Coco, G., Wysocki, R., Lerner, G. A., Rader, E., ... & Kennedy, B. (2019). The
640 heating of substrates beneath basaltic lava flows. Bulletin of Volcanology, 81(11), 1-14.
641 Vélez, M. I., Blessent, D., Córdoba, S., López-Sánchez, J., Raymond, J., & Parra-Palacio, E. (2018). Geothermal
642 potential assessment of the Nevado del Ruiz volcano based on rock thermal conductivity measurements
643 and numerical modeling of heat transfer. Journal of South American Earth Sciences, 81, 153-164.
644 Wadsworth, F. B., Llewellin, E. W., Vasseur, J., Gardner, J. E., & Tuffen, H. (2020). Explosive-effusive volcanic
645 eruption transitions caused by sintering. Science Advances, 6(39), eaba7940.
646 Weydt, L. M., Ramírez-Guzmán, Á. A., Pola, A., Lepillier, B., Kummerow, J., Mandrone, G., ... & Sass, I. (2021).
647 Petrophysical and mechanical rock property database of the Los Humeros and Acoculco geothermal fields
648 (Mexico). Earth System Science Data, 13(2), 571-598.
649 Whittington, A. G., Hofmeister, A. M., & Nabelek, P. I. (2009). Temperature-dependent thermal diffusivity of the
650 Earth's crust and implications for magmatism. Nature, 458(7236), 319-321.
651 Wooster, M. J., & Rothery, D. A. (1997). Thermal monitoring of Lascar Volcano, Chile, using infrared data from
652 the along-track scanning radiometer: a 1992–1995 time series. Bulletin of Volcanology, 58(7), 566-579.
653 Wooster, M. J., Wright, R., Blake, S., & Rothery, D. A. (1997). Cooling mechanisms and an approximate thermal
654 budget for the 1991–1993 Mount Etna lava flow. Geophysical Research Letters, 24(24), 3277-3280.
655 Wright, R., & Flynn, L. P. (2004). Space-based estimate of the volcanic heat flux into the atmosphere during 2001
656 and 2002. Geology, 32(3), 189-192.
657 Wright, R., Flynn, L. P., Garbeil, H., Harris, A. J., & Pilger, E. (2004). MODVOLC: near-real-time thermal
658 monitoring of global volcanism. Journal of Volcanology and Geothermal Research, 135(1-2), 29-49.
659 Zhang, N., & Wang, Z. (2017). Review of soil thermal conductivity and predictive models. International Journal
660 of Thermal Sciences, 117, 172-183.
661 Zimmerman, R. W. (1989). Thermal conductivity of fluid-saturated rocks. Journal of Petroleum Science and
662 Engineering, 3(3), 219-227.